

Rotating saddle trap as Foucault’s pendulum.

O.N. Kirillov ¹, M. Levi ²

1 Helmholtz-Zentrum Dresden-Rossendorf, P.O. Box 510119, D-01314 Dresden, Germany

2 Department of Mathematics, Pennsylvania State University, University Park, PA 16802, USA.

Abstract

One of the many surprising results found in the mechanics of rotating systems is the stabilization of a particle in a rapidly rotating planar saddle potential. Besides the counterintuitive stabilization, an unexpected precessional motion is observed. In this note we show that this precession is due to a Coriolis-like force caused by the rotation of the potential. To our knowledge this is the first example where such force arises in an inertial reference frame. We also propose an idea of a simple mechanical demonstration of this effect.

Introduction.

According to Earnshaw’s theorem an electrostatic potential cannot have stable equilibria, i.e. minima, since such potentials are harmonic functions. The theorem does not apply, however, if the potential depends on time; in fact, the 1989 Nobel Prize in physics was awarded to W. Paul [1] for his invention of the trap for suspending charged particles in an oscillating electric field. Paul’s idea was to stabilize the saddle by “vibrating” the electrostatic field, by analogy with the so-called Stephenson-Kapitsa pendulum [2, 3, 4, 5, 6] in which the upside-down equilibrium is stabilized by vibration of the pivot. Instead of vibration, the saddle can also be stabilized by rotation of the potential (in two dimensions); this has been known for nearly a century: as early as 1918, L.E.J. Brouwer (1881–1966), one of the authors of the fixed point theorem in topology, considered stability of a heavy particle on a rotating slippery surface, [7, 8, 9]. Brouwer derived the equations of motion in [7, 8]; the derivation took over 3 pages. He then linearized the equations by discarding quadratic and higher order terms in position and velocity. The resulting *linearized* equations in the *stationary* frame are [12, 13]

$$\begin{aligned}\ddot{x} + x \cos 2\omega t + y \sin 2\omega t &= 0, \\ \ddot{y} + x \sin 2\omega t - y \cos 2\omega t &= 0,\end{aligned}\tag{1}$$

where t is dimensionless time related to the dimensional time \hat{t} via $t = \hat{t}\Omega/\Omega_0$, $\Omega_0 = \sqrt{g/r}$,¹ and where ω is the dimensionless angular velocity given by $\omega = \Omega/\Omega_0$.

Equations (1) look even nicer in vector form:

$$\ddot{\mathbf{x}} + S(\omega t)\mathbf{x} = \mathbf{0},\tag{2}$$

¹Note that Ω_0 is the frequency of small oscillations of the particle along the x -direction on the *non-rotating* saddle. Thus our dimensionless t measures time in the units of the period of the above mentioned oscillations.

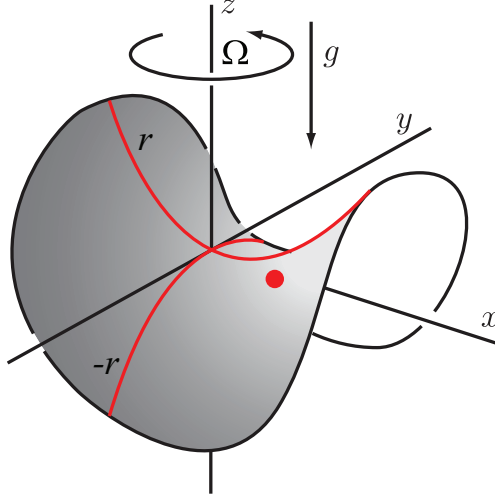


Figure 1: A unit mass on a saddle [7, 8, 9].

where

$$S(\omega t) = \begin{pmatrix} \cos 2\omega t & \sin 2\omega t \\ \sin 2\omega t & -\cos 2\omega t \end{pmatrix}. \quad (3)$$

We note that these equations are written in the stationary frame; Brouwer actually derived the corresponding equations in a frame rotating with the saddle ([7, 8, 9]). The equations (1), when written in the rotating frame, acquire the Coriolis and the centrifugal forces, but lose time-dependence since the saddle appears stationary in the co-rotating frame; the equivalence of the autonomous linear equations of Brouwer and the time-periodic equations (1) is well-known, see e.g. [13, 14, 15].

We now describe another context in which (1) appear.

A particle in a rotating potential. The same equations (1) - (2) arise also in a different context: they govern the motion of a unit mass in the *plane* under the influence of a potential force given by the rotating saddle potential – namely, the potential whose graph is obtained by rotating the graph of $z = \frac{1}{2}(x^2 - y^2)$ around the z -axis with angular velocity ω . This planar problem is related to, but is different from that of Figure 1. Physically, such a problem arises, for instance, in the motion of a charged particle in a rotating electrostatic potential, as discussed in [12].

Brouwer’s particle vs. a particle in a rotating potential. If the graph of the saddle surface in Figure 1 is given by a function $z = f(x, y, t)$, then the potential energy of the unit point mass on the surface is $U(x, y, t) = gf(x, y, t)$. If we now take the same function U as the potential energy of a particle that lives in the *plane*, we get a problem related to Brouwer’s, but not an equivalent one. To note just one aspect of the difference between the two problems, note that, unlike a particle in the plane, a particle on the surface feels centrifugal velocity-dependent forces due to the constraint to the surface. For the motions near the equilibrium these forces are quadratically small (as we will explain shortly and as was shown by Brouwer), and they disappear in the linearization. And if U itself happens to be quadratic in x and y (as it is in our case, as discussed in the next section on the derivation of (1)), then the equations for the two problems are the same.

A particle on the surface vs. a particle in a potential. We would like to add a general remark on the difference between two similar problems: a particle on a surface $z = f(x, y, t)$ in a constant gravitational field on the one hand, and a particle in the plane with a potential $U(x, y) = gf(x, y, t)$ on the other. The two systems have the same potential energy – this is the similarity. But here is the difference: the kinetic energy for the particle in the planar potential is simply $K_{\text{plane}} = \frac{1}{2}(\dot{x}^2 + \dot{y}^2)$, while

$$2K_{\text{surface}} = (1 + f_x^2)\dot{x}^2 + 2f_x f_y \dot{x}\dot{y} + (1 + f_y^2)\dot{y}^2;$$

here f_x and f_y denote partial derivatives of the height function f , is a much more complicated expression. However, since at the equilibrium $f_x = f_y = 0$, these derivatives are small near an equilibrium, and therefore $K_{\text{surface}} \approx K_{\text{plane}}$ there. Thus the near-equilibrium motions of the two systems are quite similar.

Precessional motion in the rotating saddle trap. It has been known since Brouwer that the motion of the particle on the saddle is stabilized for all sufficiently high ω [15, 17]. An illustration of a similar (but not equivalent) counterintuitive effect consists of a ball placed on a saddle surface rotating around the vertical axis and being in stable equilibrium at the saddle point [11]. We note however that the rolling ball on a surface is a non-holonomic system, entirely different from a particle sliding on a surface [25, 31].

The particle trapped in the rotating saddle exhibits a prograde precession in the laboratory frame as illustrated in Figure 2. This means that the particle moves along an elongated trajectory that in itself slowly rotates in the laboratory frame with the angular velocity ω_p in the same sense as the saddle. Up to now this precession has been explained by analyzing explicit solutions of the linearized equations ([10, 11, 12]), leaving the underlying cause of this precession somewhat mysterious.

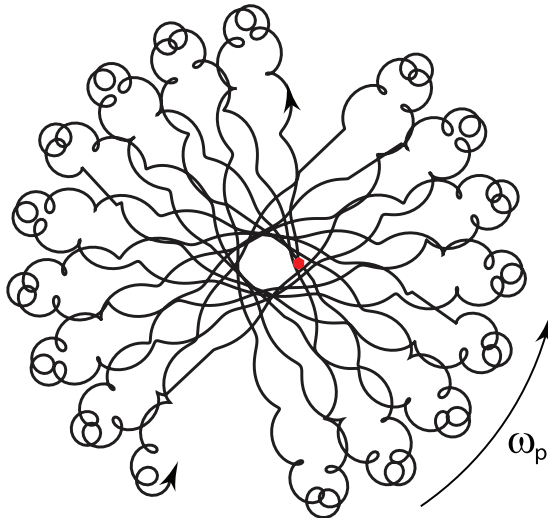


Figure 2: Prograde precession of a particle on a rotating saddle in the non-rotating frame for large angular velocity ω calculated according to equations (1). In this illustration $\omega = 20/9 \approx 2.2$ (not even that large!).

Deriving the equations of motion.

The motion of a point unit mass $\mathbf{x} = (x, y)$ in any time-dependent potential $U(x, y, t)$ is given by

$$\ddot{\mathbf{x}} = -\nabla U(\mathbf{x}, t) \quad (4)$$

(the gradient here is taken with respect to the (x, y) -coordinates). The graph of our $U(\mathbf{x}, t)$ is obtained by rotating the graph of $U_0(x, y) = \frac{1}{2}(x^2 - y^2)$, and we must (i) find the expression for this rotated potential $U(\mathbf{x}, t)$, and (ii) compute ∇U – hopefully in an elegant way, without brute force.

The answer to (i) is simply

$$U(\mathbf{x}, t) = U_0(R^{-1}\mathbf{x}), \quad (5)$$

where $R = R(\omega t)$ denotes the rotation through the angle ωt around the origin (counterclockwise if $t > 0$) and is given by the matrix

$$R = R(\omega t) = \begin{pmatrix} \cos \omega t & -\sin \omega t \\ \sin \omega t & \cos \omega t \end{pmatrix}; \quad (6)$$

Figure 3 explains why: Imagine looking down upon the graph of $U(\mathbf{x}, t)$, Figure 3(A),

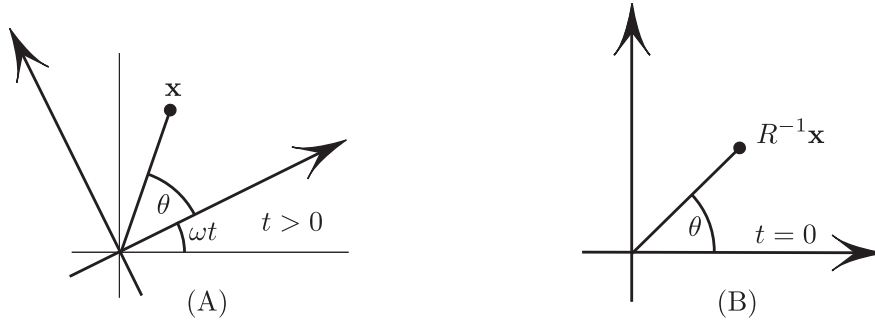


Figure 3: Explanation of (5).

focusing on a point \mathbf{x} ; let us now rotate the graph *together with* the point \mathbf{x} clockwise by angle ωt , thereby turning the graph into the graph of U_0 ; the result is shown in (B). Since the graph and the point \mathbf{x} rotated together, the height above \mathbf{x} remained unchanged – exactly what (5) says!

(ii) to find ∇U we could write (5) in terms of x and y and then differentiate, but here is a more elegant mess-avoiding way: let us write $U_0(\mathbf{x}) = \frac{1}{2}(x^2 - y^2)$ as the dot product:

$$U_0(\mathbf{x}) = \frac{1}{2}(\rho\mathbf{x}, \mathbf{x}), \quad \text{where } \rho = \text{diag}(1, -1) \quad (7)$$

(note that ρ is the mirror reflection in the y -axis), and use this in (5):

$$U(\mathbf{x}, t) = \frac{1}{2}(\rho R^{-1}\mathbf{x}, R^{-1}\mathbf{x}) = \frac{1}{2}(R\rho R^{-1}\mathbf{x}, \mathbf{x}) = \frac{1}{2}(S\mathbf{x}, \mathbf{x}); \quad (8)$$

in (8) we used the fact that R is an orthogonal matrix. Multiplying out $R\rho R^{-1} = S$ gives the matrix S defined by equation (3).

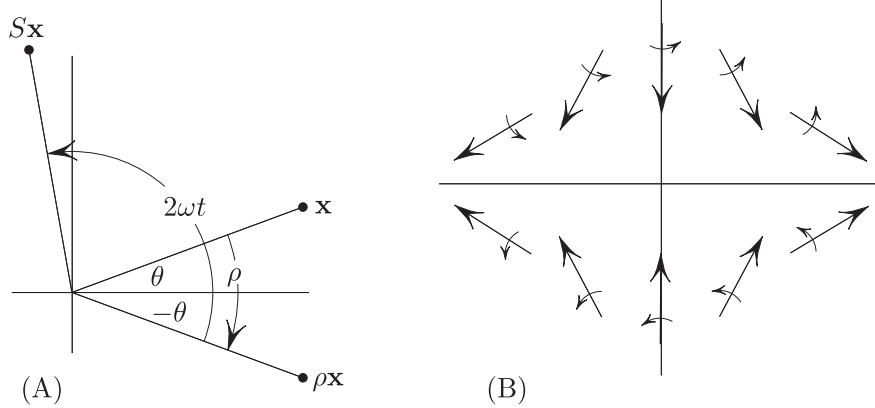


Figure 4: (A): S is a reflection followed by a rotation. (B). Another interpretation of the rotating saddle: rotating the potential with angular velocity ω amounts to rotating each arrow of the vector field $\langle x, -y \rangle$ with angular velocity 2ω .

Now for any symmetric matrix S , one has $\nabla(S\mathbf{x}, \mathbf{x}) = 2S\mathbf{x}$, as one can see with almost no computation², and we conclude

$$\nabla U(\mathbf{x}, t) = S\mathbf{x}; \tag{9}$$

Equation of motion (4) turns into (2), as claimed.

A “spinning arrows” interpretation of rotating saddle. Note that $S(\omega t)$ is a composition of the reflection with respect to the x -axis and the counterclockwise rotation through angle $2\omega t$, Figure 4(A). Therefore, for a *fixed* \mathbf{x} and increasing t , the vector $S(\omega t)\mathbf{x}$ rotates counterclockwise with angular velocity 2ω . This leads to the following nice geometrical interpretation of the governing equations (1)–(2). The force field $-S(\omega t)\mathbf{x}$ in our equations (2) can be thought of in the following way, Figure 4(B). Starting with the stationary saddle vector field $\langle x, -y \rangle$, we rotate each arrow of this field with angular velocity 2ω counterclockwise; the result is our time-dependent vector field $-\nabla U(\mathbf{x}, t) = -S(\omega t)\mathbf{x}$.

Applications, connections to other systems.

Before getting to the point of this note, we mention that equations (1) arise in numerous applications across many seemingly unrelated branches of classical and modern physics [11, 13, 14, 15]; here is a partial list. They describe stability of a mass mounted on a non-circular weightless rotating shaft subject to a constant axial compression force [16, 17], in plasma physics they appear in the modeling of a stellatron – a high-current betatron with stellarator fields used for accelerating electron beams in helical quadrupole magnetic fields [10, 13, 18]. In quantum optics, equations (1) originate in the theory of rotating radio-frequency ion traps [12]. In celestial mechanics the rotating saddle equations describe linear stability of the triangular Lagrange libration points L_4 and L_5 in the restricted circular three-body problem [19, 20, 21]. In atomic physics the stable

²Indeed, the definition of the gradient of a function f states: $(\nabla f(\mathbf{x}), \mathbf{v}) \stackrel{def}{=} \frac{d}{ds} f(\mathbf{x} + s\mathbf{v})_{s=0}$ for all vectors \mathbf{v} . In our case, $f(\mathbf{x}) = (S\mathbf{x}, \mathbf{x})$ and $\frac{d}{ds} f(\mathbf{x} + s\mathbf{v})_{s=0} = (2S\mathbf{x}, \mathbf{v})$; comparing this with the left-hand side of the definition proves $\nabla(S\mathbf{x}, \mathbf{x}) = 2S\mathbf{x}$.

Lagrange points were produced in the Schrödinger-Lorentz atomic electron problem by applying a circularly polarized microwave field rotating in synchrony with an electron wave packet in a Rydberg atom [21]. This has led to a first observation of a non-dispersing Bohr wave packet localized near the Lagrange point while circling the atomic nucleus indefinitely [22]. Recently, the rotating saddle equations (1) reappeared in the study of confinement of massless Dirac particles, e.g. electrons in graphene [23]. Interestingly, stability of a rotating flow of a perfectly conducting ideal fluid in an azimuthal magnetic field possesses a mechanical analogy with the stability of Lagrange triangular equilibria and, consequently, with the gyroscopic stabilization on a rotating saddle [24].

The result: a “hodograph” transformation

The main point of this note is to show that the rapid rotation of the saddle gives rise to an unexpected Coriolis-like or magnetic-like force *in the laboratory frame*; it is this force that is responsible for prograde precession. To our knowledge this is the first example where the Coriolis-like force arises in the inertial frame.

To state the result we assign, to any motion $\mathbf{x} = \mathbf{x}(t)$ satisfying (2), its “guiding center”, or “hodograph”³

$$\mathbf{u} = \mathbf{x} - \frac{\varepsilon^2}{4} S(\omega t)(\mathbf{x} - \varepsilon J \dot{\mathbf{x}}), \quad (10)$$

where $\varepsilon = \omega^{-1}$ and where J is the counterclockwise rotation by $\pi/2$:

$$J = \begin{pmatrix} 0 & -1 \\ 1 & 0 \end{pmatrix}. \quad (11)$$

We discovered that for large ω , i.e. small ε , the guiding center has a very simple dynamics:

$$\ddot{\mathbf{u}} - \frac{\varepsilon^3}{4} J \dot{\mathbf{u}} + \frac{\varepsilon^2}{4} \mathbf{u} = O(\varepsilon^4); \quad (12)$$

that is, ignoring the ε^4 -terms, \mathbf{u} behaves as a particle with a Hookean restoring force $-\frac{\varepsilon^2}{4} \mathbf{u}$ and subject to the Coriolis- or magnetic- like force $\frac{\varepsilon^3}{4} J \dot{\mathbf{u}}$. Figure 5 shows a typical trajectory of the truncated equation

$$\ddot{\mathbf{u}} - \frac{\varepsilon^3}{4} J \dot{\mathbf{u}} + \frac{\varepsilon^2}{4} \mathbf{u} = 0. \quad (13)$$

This is in fact the motion of a Foucault pendulum, and just as in the Foucault pendulum [26] the Coriolis-like term is responsible for prograde precession of \mathbf{u} and thus of its “follower” \mathbf{x} .

³The conventional hodograph transformation involves the derivatives of the unknown function. Hamilton referred to the path of the tip of the velocity vector of an orbiting planet as the hodograph (the word is a combination of the Greek words for *path* and for *trace, or describe*). Following Hamilton, in meteorology the hodograph is the trajectory of the tip of the velocity vector; in partial differential equations, Legendre’s hodograph transformation involves partial derivatives. We refer to (10) as a hodograph transformation since \mathbf{u} is a certain mixture of position and velocity.

Angular velocity of precession in (13) compared to earlier results. Angular velocity of precession of solutions of the Foucault-type equation (13) turns out to be $\omega_p = \varepsilon^3/8$. Indeed, writing the equation in the frame rotating with angular velocity ω_p gives rise to a Coriolis term and a centrifugal term, and the system in that frame becomes

$$\ddot{\mathbf{z}} + 2\omega_p J \dot{\mathbf{z}} - \frac{\varepsilon^3}{4} J \dot{\mathbf{z}} + \frac{\varepsilon^2}{4} \mathbf{z} + \omega_p^2 \mathbf{z} = 0. \quad (14)$$

With the above value of ω_p , the second and the third terms cancel, and the resulting system

$$\ddot{\mathbf{z}} + (\varepsilon^2/4 + \varepsilon^6/64) \mathbf{z} = 0 \quad (15)$$

exhibits no precession (all solutions are simply ellipses). We conclude that $\varepsilon^3/8$ is indeed the angular velocity of precession of \mathbf{u} . This simple expression fits with the earlier results and also gives the precession speed for the near-equilibrium motions of Brouwer’s particle, as we show next.

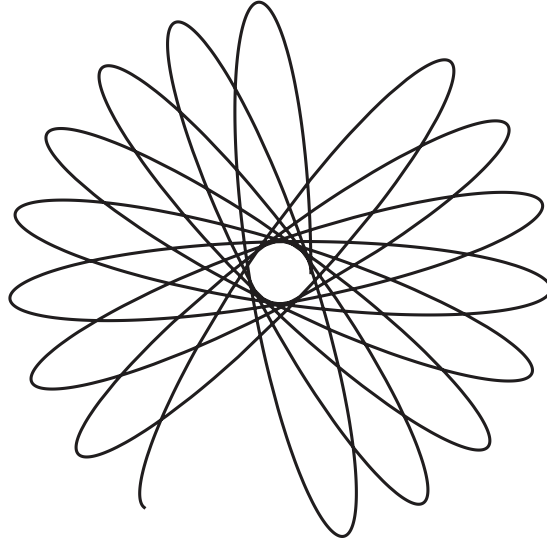


Figure 5: The motion of the “guiding center”, governed by (13), is the same as that of a Foucault pendulum. Here $\varepsilon = 0.45$.

The equations of a rotating radio-frequency ion trap obtained in [12] reduce to our equations (1) with $\varepsilon = \omega^{-1} = \sqrt{2q}$ after the re-scaling of time: $t = \tau\sqrt{2q}$, where t is the dimensionless time in (1) and τ and q represent here, respectively, the dimensionless time and a dimensionless parameter of the trap in [12]. Calculating the angle of precession $\omega_p t$, we find

$$\omega_p t = \frac{\varepsilon^3}{8} t = \frac{\varepsilon^3}{8} \sqrt{2q} \tau = \frac{4q^2}{8} \tau = \frac{q^2}{2} \tau, \quad (16)$$

which yields the precession rate obtained by Hasegawa and Bollinger [12]:

$$\omega_p^{HB} = \frac{q^2}{2}. \quad (17)$$

Similarly, the dimensional precession frequency of the particle in Figure 1 is:

$$\Omega_p = \frac{g^2}{8r^2\Omega^3}. \quad (18)$$

A Coriolis-like force in the inertial frame. If $\frac{\varepsilon^3}{4}J\dot{\mathbf{u}}$ were a true Coriolis force, it would have been due to the rotation of the reference frame with angular velocity $\frac{\varepsilon^3}{8}$ – but our frame is inertial. Alternatively, one can think of $\frac{\varepsilon^3}{4}J\dot{\mathbf{u}}$ as the Lorentz force exerted on a charge (of unit mass and of unit charge) in constant magnetic field $B = \frac{\varepsilon^3}{4}$ perpendicular to the plane. Rapid rotation of the saddle gives rise to a virtual pseudo-magnetic force (cf. [27, 28, 29]); as one implication, the asteroids in the vicinity of Lagrange triangular equilibria behave like charged particles in a weak magnetic field, from the inertial observer’s point of view.

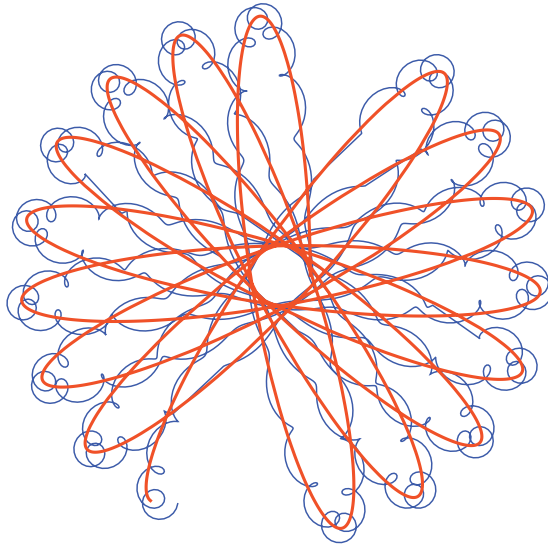


Figure 6: A trajectory of the guiding center \mathbf{u} governed by (13) (in red) tracking the corresponding trajectory \mathbf{x} governed by (2). The view is in the inertial frame. $\varepsilon = 0.45$.

A numerical illustration. Figure 6 shows a solution \mathbf{x} alongside its “guiding center” \mathbf{u} . We note, as a side remark, that near the origin the solution follows the trajectory of the guiding center rather closely, reflecting the fact that oscillatory micromotion is small near the origin, as is clear from the governing equations (1).

We discovered the hodograph transformation (10) via a somewhat lengthy normal form argument [5, 6] which, due to its length, will be presented elsewhere. Nevertheless, once the transformation (10) has been produced, the statement (12) can be verified directly by substituting (10) into (2); we omit the routine but slightly lengthy details, but give a geometrical view of this transformation.

A geometrical view of the hodograph transformation. Our result says, in effect, that the “jiggle” term

$$\frac{\varepsilon^2}{4}S(\omega t)(\mathbf{x} - \varepsilon J\dot{\mathbf{x}}) \tag{19}$$

in (10), when subtracted from \mathbf{x} , leaves a smooth motion.⁴ Figure 7 gives a geometrical view of this term. It is still an open problem to find a simple heuristic explanation

⁴as far as the powers up to ε^3 are concerned.

of choice of the term $-\varepsilon J\dot{\mathbf{x}}$ in (10). Finding a heuristic explanation of the “magnetic” term $\frac{\varepsilon^3}{4}J\dot{\mathbf{u}}$ remains an open problem as well.

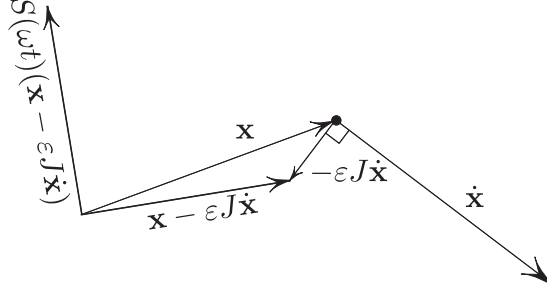


Figure 7: A geometrical representation of the “jiggle” term $S(\omega t)(\mathbf{x} - \varepsilon J\dot{\mathbf{x}})$ (without the $\varepsilon^2/4$ factor) in the hodograph transformation. One should “read” the figure in the following order: $x \mapsto \dot{x} \mapsto -\varepsilon J\dot{x} \mapsto x - \varepsilon J\dot{x} \mapsto S(x - \varepsilon J\dot{x})$. A geometrical interpretation of S is shown in Figure 4(A).

Validity of the truncation. Our result says that the fictitious particle \mathbf{u} , which shadows the solution \mathbf{x} , is subject to two forces $-(\varepsilon^3/4)\dot{\mathbf{u}} - (\varepsilon^2/4)\mathbf{u}$, plus a smaller $O(\varepsilon^4)$ -force.

What is the cumulative effect of this force? One can show, using standard results of perturbation theory, that neglecting the $O(\varepsilon^4)$ -term causes the deviation less than $c_1\varepsilon^3$ over the time $|t| < c_2\varepsilon^{-2}$ for some constants c_1, c_2 , for all ε sufficiently small. As it often happens with rigorous results, this one is overly pessimistic: computer simulations show that “sufficiently small” is actually not that small: for example, $\varepsilon = 0.45$ in Figure 6. In fact, the reason for such an unexpectedly good agreement is the fact that the error on the right-hand side is actually $O(\varepsilon^6)$ – two orders better than claimed, as follows from an explicit computation by Michael Berry, [30]. We do not focus on the analysis of higher powers of ε because it would only add *higher-order* corrections to the coefficients on the left-hand side of (12), without affecting our main point (namely, that an unexpected Coriolis-like force appears).⁵

A proposed experiment.

Figure 8 illustrates a possible mechanical implementation of the rotating saddle trap (cf. [16, 17]). As we had mentioned in the introduction, a ball rolling on the rotating saddle surface [11] is *not* the right physical realization of the rotating saddle trap because

⁵According to M. Berry’s computation [30] based on explicit solution of (1), replacing the coefficient $\varepsilon^2/4$ in (13) by

$$\frac{\varepsilon^2}{4} \left(1 + \frac{3}{16}\varepsilon^4 + \frac{11}{128}\varepsilon^8 + \dots \right) = -\frac{(1 - \sqrt{1 - \varepsilon^2})(1 - \sqrt{1 + \varepsilon^2})}{\varepsilon^2}, \quad (20)$$

and replacing the coefficient $\varepsilon^3/4$ by

$$\frac{\varepsilon^3}{4} \left(1 + \frac{5}{16}\varepsilon^4 + \frac{21}{128}\varepsilon^8 + \dots \right) = \frac{2}{\varepsilon} - \frac{\sqrt{1 - \varepsilon^2} + \sqrt{1 + \varepsilon^2}}{\varepsilon}. \quad (21)$$

yields the equation for the exact guiding center (the expression for which is then given by (10) which includes higher order terms).

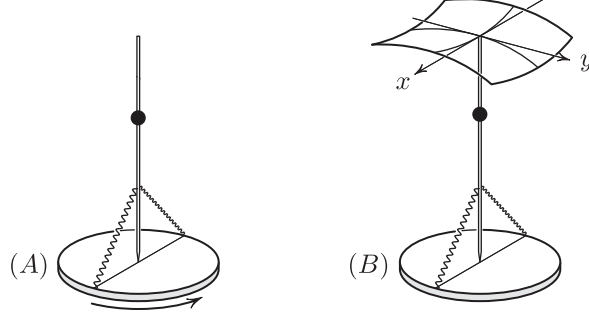


Figure 8: A possible mechanical realization of the rotating saddle trap. Here x, y are the angular variables, and the graph of the potential energy in terms of the angular variables x, y is shown.

(i) the friction is very hard to eliminate, and, perhaps more importantly, because the rolling ball does not behave as a sliding particle. In fact, the rolling ball can be stable even *on top* of a sphere rotating around its vertical diameter [31]!

A light rod with a massive ball in Figure 8 is essentially an inverted spherical pendulum; the sharpened end of the rod, resting on the center of the platform, acts as a ball joint with the horizontal plane. The springs are attached to the rod.⁶ The height of the ball is adjustable, like in a *metronome*. If the ball is placed sufficiently low then the two springs will stabilize the pendulum in the x -direction, Figure 8(B),⁷ and the potential acquires a saddle shape (since the y -direction is unstable):

$$U_0(x, y) = \frac{1}{2} (ax^2 - by^2), \quad (22)$$

with $a, b > 0$, ignoring higher powers of x, y . Here $b = g/L$, where L is the distance from the ball to the sharpened end of the rod. In the next paragraph we suggest a simple way to adjust L to make the two curvatures equal: $a = b$, so that the linearized equations become

$$\ddot{\mathbf{x}} + bS(\Omega t)\mathbf{x} = 0, \quad b = \frac{g}{L} \quad (23)$$

a rescaled version of (1). By rescaling the physical time t to the dimensionless time $\tau = \sqrt{at}$, and introducing

$$\omega = \Omega/\sqrt{a}, \quad (24)$$

we transform the above equation into the dimensionless form (1) (after renaming τ back to t), which is stable if $\omega > 1$ [7, 15, 17]. Now $a = b = g/L$, where L is the distance from the mass to the ball joint, and (24) gives us the length

$$L = g \left(\frac{\omega}{\Omega} \right)^2. \quad (25)$$

⁶Theoretically, we want to avoid transferring the rotation of the platform to the rotation of the rod around its long axis (thereby affecting its dynamics), and thus the attachment should, theoretically, be via some frictionless sleeve. In practice, however, this frictionless sleeve will hardly make a difference: the moment of inertia of the rod+ball around the long axis is negligible compared to the moment of inertia relative to a diameter of the platform, and thus the dynamics of the rod will be little affected by its axial rotation.

⁷here x and y are angular variables.

The 78 rpm of a vinyl record player corresponds to $\Omega \approx 8.2 \text{sec}^{-1}$, and the value $\omega \approx 2.2$ referred to in Figure 2 corresponds to the height $L \approx 71 \text{ cm}$. How short can we make the pendulum without losing stability? The cutoff length is $L \approx 14 \text{ cm}$, as follows from (25) and the fact that (1) is stable if and only if $\omega > 1$. Incidentally, large L corresponds to large ω , according to (25) (for fixed rpm). This makes intuitive sense, since a “natural” unit of time in our system is the period $2\pi\sqrt{L/g}$ of the oscillations along the stable axis of the stationary potential; for large L this period is long, and during it the rotating potential will spin many times, corresponding to large ω .

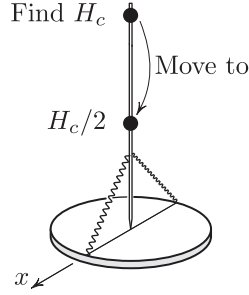


Figure 9: How to find the length for which the curvatures of the saddle are equal and opposite: $U_{xx}(0,0) = -U_{yy}(0,0)$: find by trial and error the height H_c at which the x -direction changes stability, and half H_c .

How to (easily) realize the saddle with equal principal curvatures. It may seem (as it did to us initially) that one needs to measure the stiffnesses of the springs, the various lengths in Figure 8, the mass of the ball, and then use these to compute the value of L . Instead, here is a way to avoid all this work. Referring to Figure 9, *adjust the position of the massive ball along the rod to such critical height H_c as to make the ball neutrally stable in the x -direction*: if the ball is too high, it will be unstable in the x -direction; if the ball is too low, it will be stable in the x -direction; a bisection method will quickly lead to a good approximation to H_c . Remarkably, the desired “equal curvatures” height of the ball is simply

$$L = \frac{H_c}{2}. \quad (26)$$

An explanation. The angle y satisfies the inverted pendulum equation $\ddot{y} - \frac{g}{L} \sin y = 0$, which for small angles is well approximated by

$$\ddot{y} - \frac{g}{L} y = 0. \quad (27)$$

Similarly, the linearized equation for the angle x is

$$\ddot{x} + \left(-\frac{g}{L} + \frac{k}{L^2} \right) x = 0; \quad (28)$$

L is not yet chosen and k depends on the parameters of the system, but not on L .⁸ Our goal is to find L such that the coefficients in the above equations are equal and

⁸Specifically, k depends on the springs’ stiffness, on the angle they form with the diameter in Figure 8 and on the ball’s mass (to which it is inversely proportional). But an easier way to find k is to note that $k = gH_c$, as we show below.

opposite, which amounts to asking for L satisfying $\frac{g}{L} = -\frac{g}{L} + \frac{k}{L^2}$, or

$$2Lg = k. \tag{29}$$

We now relate the unknown k to H_c . For the pendulum of the length H_c the angle x satisfies $\ddot{x} + (-\frac{g}{H_c} + \frac{k}{H_c^2})x = 0$, with the coefficient $-\frac{g}{H_c} + \frac{k}{H_c^2} = 0$ since the equilibrium is neutral; this gives

$$k = gH_c. \tag{30}$$

Substituting $H_c = 2L$ into the last equation gives (29) – precisely the condition for the equality of the coefficients in U .

Conclusion. We showed that the rapid rotation of the saddle potential creates a weak Lorentz-like, or a Coriolis-like force, in addition to an effective stabilizing potential – all in the inertial frame. We also proposed a simple experiment to demonstrate the phenomenon.

Acknowledgement Mark Levi gratefully acknowledges support by the NSF grant DMS-0605878.

References

- [1] W. Paul, Electromagnetic traps for charged and neutral particles, *Rev. Mod. Phys.*, 62, 531–540, 1990.
- [2] A. Stephenson, On an induced stability, *Phil. Mag.*, 15, 233, 1908.
- [3] P. L. Kapitsa, Pendulum with a vibrating suspension, *Usp. Fiz. Nauk*, 44, 7–15, 1951.
- [4] L. D. Landau, E. M. Lifshitz (1960). *Mechanics*. Vol. 1 (1st ed.). Pergamon Press.
- [5] M. Levi, Geometry of Kapitsa’s potentials, *Nonlinearity*, 11, 1365–1368, 1998.
- [6] M. Levi, Geometry and physics of averaging with applications, *Physica D*, 132, 150–164, 1999.
- [7] L. E. J. Brouwer, Beweging van een materieel punt op den bodem eener draaiende vaas onder den invloed der zwaartekracht, *N. Arch. v. Wisk.*, 2, 407–419, 1918.
- [8] L. E. J. Brouwer, The motion of a particle on the bottom of a rotating vessel under the influence of the gravitational force, in: H. Freudenthal (ed.), *Collected Works*, II, pp. 665–686, North-Holland, Amsterdam, 1975.
- [9] O. Bottema, Stability of equilibrium of a heavy particle on a rotating surface, *ZAMP Z. angew. Math. Phys.*, 27, 663–669, 1976.
- [10] R. M. Pearce, Strong focussing in a magnetic helical quadrupole channel, *Nuclear instruments and methods*, 83(1), 101–108, 1970.

- [11] R. I. Thompson, T. J. Harmon, M. G. Ball, The rotating-saddle trap: a mechanical analogy to RF-electric-quadrupole ion trapping? *Canadian Journal of Physics*, 80, 1433–1448, 2002.
- [12] T. Hasegawa, J. J. Bollinger, Rotating-radio-frequency ion traps, *Phys. Rev. A*, 72, 043403, 2005.
- [13] V. E. Shapiro, Rotating class of parametric resonance processes in coupled oscillators, *Phys. Lett. A*, 290, 288–296, 2001.
- [14] O. N. Kirillov, Exceptional and diabolical points in stability questions. *Fortschritte der Physik - Progress in Physics*, 61(2-3), 205–224, 2013.
- [15] O. N. Kirillov, *Nonconservative Stability Problems of Modern Physics*, De Gruyter, Berlin, Boston, 2013.
- [16] D. J. Inman, A sufficient condition for the stability of conservative gyroscopic systems, *Trans. ASME J. Appl. Mech.*, 55, 895–898, 1988.
- [17] K. Veselic, On the stability of rotating systems, *ZAMM Z. angew. Math. Mech.*, 75, 325–328, 1995.
- [18] C. W. Roberson, A. Mondelli, D. Chernin, High-current betatron with stellarator fields, *Phys. Rev. Lett.*, 50, 507–510, 1983.
- [19] M. Gascheau, Examen d’une classe d’équations différentielles et application à un cas particulier du probleme des trois corps, *Comptes Rendus*, 16, 393–394, 1843.
- [20] K. T. Alfriend, The stability of the triangular Lagrangian points for commensurability of order two, *Celestial Mechanics*, 1(3–4), 351–359, 1970.
- [21] I. Bialynicki-Birula, M. Kaliński, J. H. Eberly, Lagrange equilibrium points in celestial mechanics and nonspreading wave packets for strongly driven Rydberg electrons, *Phys. Rev. Lett.*, 73, 1777–1780, 1994.
- [22] H. Maeda, J. H. Gurian, T. F. Gallagher, Nondispersing Bohr wave packets, *Phys. Rev. Lett.*, 102, 103001, 2009.
- [23] J. Nilsson, Trapping massless Dirac particles in a rotating saddle, *Phys. Rev. Lett.*, 111, 100403, 2013.
- [24] G. I. Ogilvie, J. E. Pringle, The non-axisymmetric instability of a cylindrical shear flow containing an azimuthal magnetic field, *Mon. Not. R. Astron. Soc.*, 279, 152–164, 1996.
- [25] Ju. I. Neimark, N. A. Fufaev, *Dynamics of Nonholonomic Systems (Translations of Mathematical Monographs, V. 33)*, American Mathematical Society, Providence, RI, 2004.
- [26] A. Khein, D. F. Nelson, Hannay angle study of the Foucault pendulum in action-angle variables, *Am. J. Phys.* 61(2), 170–174, 1993.

- [27] M. V. Berry, J. M. Robbins, Chaotic classical and half-classical adiabatic reactions: geometric magnetism and deterministic friction, *Proc. R. Soc. A* 442, 659–672, 1993.
- [28] M. V. Berry, P. Shukla, High-order classical adiabatic reaction forces: slow manifold for a spin model, *J. Phys. A: Math. Theor.* 43, 045102, 2010.
- [29] M. V. Berry, P. Shukla, Slow manifold and Hannay angle for the spinning top, *Eur. J. Phys.* 32, 115–127, 2011.
- [30] M. V. Berry, Private communication, 15 February, 2015.
- [31] W. Weckesser, A ball rolling on a freely spinning turntable, *Am. J. Phys.*, 65, 736–738, 1997.